



## Experimental Study of a Funicular Concrete Beam Prototype

---

Maximilian Ororbia, Hua Chai, Yefan Zhi, Pouria Vakhshouri,  
Jorge Chacon, Joseph Yost, Mathias Bernhard,  
Fahimeh Yavartanoo, Javier Tapia, Damon Bolhassani,  
Mylene Bernard, Leon Trouset, Karolina Pajak, Blaise Waligun,  
Paul Kassabian and Masoud Akbarzadeh

EasyChair preprints are intended for rapid  
dissemination of research results and are  
integrated with the rest of EasyChair.

October 9, 2024



## Experimental study of a funicular concrete beam prototype

Maximilian E. ORORBIA<sup>\*,a</sup>, Hua CHAI<sup>a</sup>, Yefan ZHI<sup>a</sup>, Pouria VAKHSHOURI<sup>a</sup>, Jorge Huisa CHACON<sup>b</sup>, Joseph R. YOST<sup>b</sup>, Mathias BERNHARD<sup>c</sup>, Fahimeh YAVARTANOO<sup>d</sup>, Javier TAPIA<sup>d</sup>, Damon BOLHASSANI<sup>d</sup>, Mylene BERNARD<sup>e</sup>, Leon TROUSSET<sup>e</sup>, Karolina PAJAK<sup>e</sup>, Blaise WALIGUN<sup>f</sup>, Paul KASSABIAN<sup>f</sup>, Masoud AKBARZADEH<sup>a</sup>

<sup>a</sup> Polyhedral Structures Laboratory, Weitzman School of Design, University of Pennsylvania  
Pennovation Center, 3401 Grays Ferry Ave. Philadelphia, PA, 19146, USA

\*mororbia@upenn.edu

<sup>b</sup> Villanova University, Villanova, PA, USA

<sup>c</sup> ETH, Zurich, Switzerland

<sup>d</sup> The City College of New York, New York City, NY, USA

<sup>e</sup> SIKA, Zurich, Switzerland

<sup>f</sup> Simpson, Gumpertz, & Heger (SGH), Boston, MA, USA

### Abstract

This work presents the design and construction of a concrete 3D-printed, post-tensioned funicular beam prototype as well as the experimental test results of subjecting the beam to four-point bending. The beam is designed as a combined compression and tension funicular system with minimized mass and optimized reinforcement. Periodic anticlastic surfaces are embedded within the thrust network to inherently increase geometric stiffness. In consideration of construction, sustainability, and recyclability, the beam is designed as a modular system, consisting of nine individual segments, where each segment is 3D-printed using a multi-component concrete mix with a multi-axis industrial robot arm. Post-tensioning the nine individual segments together with ungrouted steel cables forms the beam. Beneficially, the beam can be readily disassembled and recycled since the concrete and steel can be separated easily from each other. To understand the structural performance, and how both the funicular load path and the geometric stiffness work in tandem, a four-point bending test was conducted. The experimental test provides insights on, and captures the complexities associated with, the overall design, fabrication, and construction, and reveals the flexural behavior and mode of failure. Design, fabrication, construction, and structural testing processes and setups are outlined and discussed. This study establishes a foundational basis that will be used to further develop and enhance such structural systems for more sustainable construction practices in the future.

**Keywords:** Funicular beam, embedded periodic anticlastic surfaces, concrete 3D-printing, post-tensioning, four-point bending test

### 1. Introduction

The design, fabrication, construction, and structural testing of a funicular concrete beam prototype are presented in this work. Designed using a comprehensive computational framework [1], the beam prototype pushes the boundaries of conventional construction practices by combining and developing upon existing and new methods and technologies. The beam's design takes advantage of post-tensioning and the geometric capabilities that concrete 3D printing provides by placing minimal, tension-only reinforcement directly along the identified load paths and embedding periodic anticlastic surfaces to increase

stiffness. The fabrication and assembly approaches presented enable faster construction times, eliminate use of formwork, and allow for recyclability of materials. Since the beam is designed and assembled as a modular system, with ungrouted post-tensioning cables compressing the segments together, the beam at its end-of-service life can be disassembled where both the concrete and steel can be efficiently and entirely separated from each other to be recycled.

To assess the beam's performance and observe its behavior a four-point bending test was performed. Three cycles of the four-point bending test were conducted to determine the ultimate load-bearing capacity of the beam and observe its behavior under increased loads. Beyond evaluating the beam's material strength and structural stiffness, this test provided valuable insights into various aspects of the design, fabrication, and construction processes. The overall effectiveness of the design and fabrication strategies as well as the interaction between construction materials are assessed and used to inform future development.

This paper is organized as follows: Section 2 describes the design process, considerations, and specifications of the funicular beam together with the experimental fabrication procedure incorporating robotic concrete 3D printing, slicing, developing toolpaths, and segmentation. Section 3 comprehensively addresses the post-tensioning and assembly process, discussing approaches to increase the structural efficiency and resiliency of the funicular beam. Section 4 describes the structural test setup in detail, describes each cycle of the test results and observations, and associates the test results with the design, fabrication, and construction. Concluding remarks are made in Section 5 as well as insights and understanding helpful for future investigations.

## **2. Design and fabrication**

The funicular concrete beam prototype was designed using a comprehensive computational method that combines both form-finding and volumetric modeling approaches while incorporating fabrication considerations [1]. Initially, a compression-tension combined funicular geometric model is developed [2]. This geometry is then used to inform the geometric transformation applied to the periodic anticlastic surfaces for embedding. Channels are incorporated in the design for housing post-tensioning cables, located primarily where tensile forces are determined in the geometric model. Concrete 3D printing constraints are included throughout the design process through the use of slicing and toolpath optimization algorithms. The comprehensive computational approach used for the funicular beam prototype effectively results in a structure that can be prefabricated with reduced construction materials, including reinforcement, and can be concrete 3D-printed, thus eliminating the need for formwork and waste generated from conventional cast concrete construction.

### **2.1. Geometric form-finding and volumetric modeling**

Polyhedral Graphic Statics (PGS) [3, 4], a geometry-based structural design method, was used for the form-finding process. Form and force diagrams were generated given specific boundary conditions, including support conditions and applied load locations, Figure 1(a), accounting for an unfactored live load of  $5 \text{ kN/m}^2$  [5]. The corresponding force diagram load network was optimized to have constant tension forces for the application of post-tensioning. With a final form diagram generated, initial polyhedral, unit cells were defined for materialization. Periodic anticlastic surfaces [6, 7], specifically the "Diamond" triply periodic minimal surface (TPMS) geometry, were embedded in the unit cells, Figure 1(b). Materialization through the diamond TPMS was selected since the geometry could be transformed to match the principal stress directions and served as a more suitable candidate considering 3D printing constraints, particularly to reduce severe, unprintable overhangs. Overall, periodic anticlastic surfaces can enhance the structural form's geometric stiffness and provide internal channels for the post-tensioned cables re-

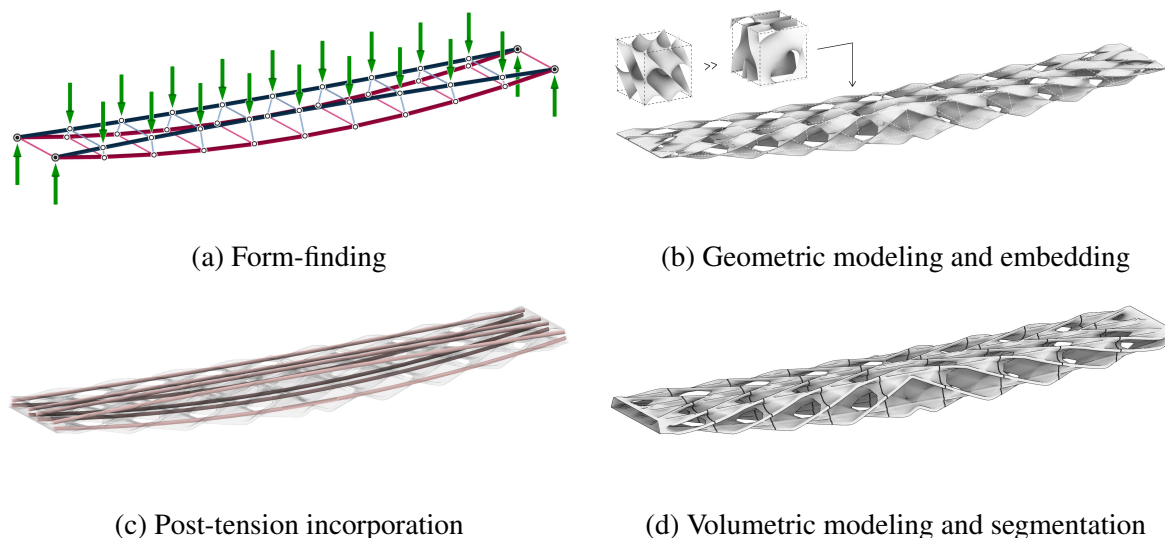


Figure 1: Computational design workflow adapted from [1]. The workflow includes multiple phases: (a) structural design and load path optimization using Polyhedral Graphic Statics, (b) geometric modeling and embedding of anticlastic periodic surfaces optimized with minimal overhangs for 3D-printing, (c) incorporation of post-tensioning cables along primary load paths, and (d) volumetric geometry generation and segmentation development considering concrete 3D printing constraints.

sulting in a fully integrated material-structural system. Signed distance function modeling [8, 9, 10] was used as a final step in the design workflow to combine the funicular form and embedded anticlastic surfaces into a smooth, unified model for fabrication.

## 2.2. Concrete 3D printing

Due to the geometric complexity of the embedded anticlastic surfaces, conventional cast-in-place concrete molding using formwork was not feasible to construct the beam. Either bespoke, one-time-use forms would have to be constructed and partially left as a part of the structure or demolished and removed after curing, increasing the amount of waste. Hence, to fabricate the beam without formwork, concrete 3D printing technology was utilized. In particular, a concrete-printing end-of-arm tool attached to an industrial 6-axis robot arm was used to manufacture the beam. A multi-component concrete recipe consisting of mortar powder, plasticizer, water, and accelerator was mixed and used as the printing material.

Constrained by factors such as the robot's workspace and the slump behavior of soft material under its self-weight, the complete fabrication of a singular 4.5-meter-long beam by the standard continuous printing method was not possible. Overcoming these constraints necessitated the structural segmentation of the beam alongside the implementation of slicing and toolpath optimization. The beam was segmented into nine pieces, each able to be printed and later, after curing, assembled utilizing post-tensioning cables threaded through the embedded channels. The angle between the segmentation planes was determined to ensure that, similar to an inverted stereotomic interlocking vault, the pieces would rest on each other and interlock geometrically. Moreover, this segmented configuration offers advantages in terms of end-of-life recyclability and reuse, as disassembly can be achieved without resorting to demolition.

To convert the geometry into toolpaths for robotic printing, each segment (Figure 2a) is sliced by non-parallel planes that ensure the concrete layers are printed perpendicular to the compression forces de-

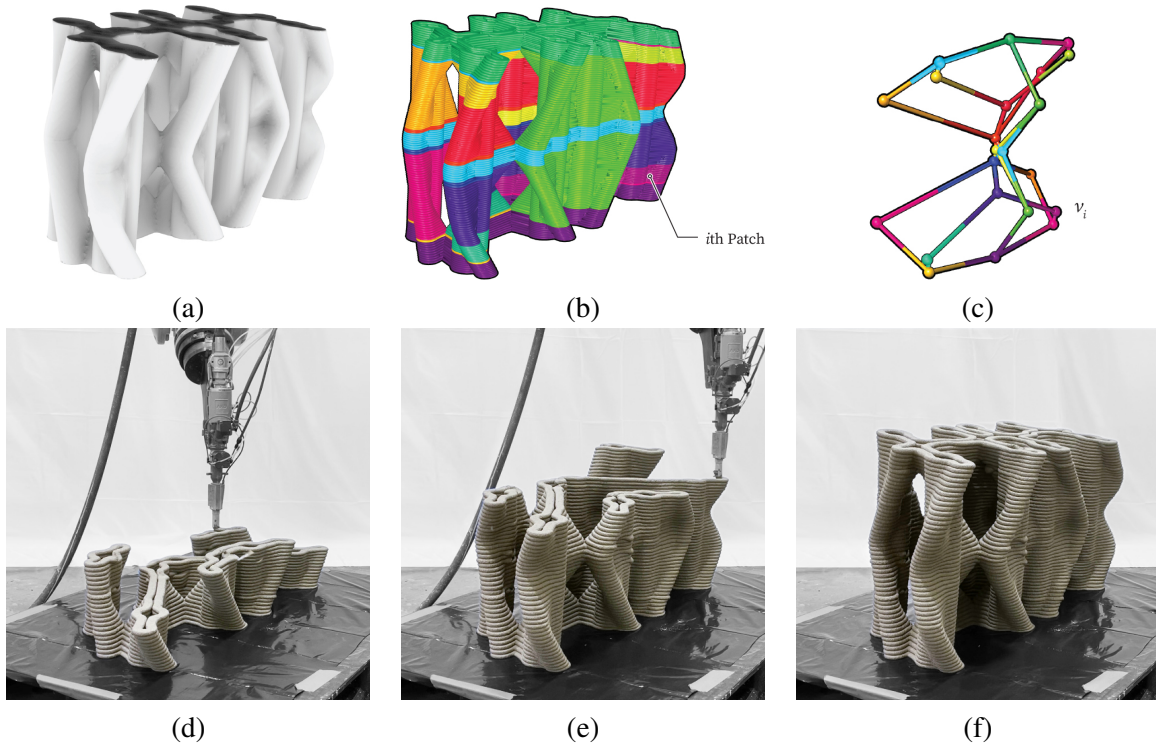


Figure 2: Fabrication process, including both digital and physical, for the funicular beam prototype's middle segment. Starting with the (a) digital model of the segment, (b) toolpath patches and (c) the dependency graph were solved to help determine the printing scheme. Images (d), (e), and (f) are of different stages of the printing process. Multiple printing islands with different heights can be identified in (d) and (e). The final printed segment (f) matches the digital model (a).

terminated using PGS. The toolpaths are then divided into patches according to the topology of the input such that each  $i$ th patch represents one continuous island to print (Figure 2b). A dependency graph is also developed to visualize the constraint in printing order between the patches,  $v_i$  (Figure 2c). Based on the patch and dependency information, a greedy algorithm subdivides and organizes the patches to prepare continuous, collision-free toolpaths resulting in a minimal number of printing start-and-stops. Additionally, an offset method was used to reconfigure the toolpaths locally, alleviating extreme overhangs.

Each segment of the beam took approximately 20 minutes to print. The concrete printing process for the middle module of the funicular beam is shown in Figure 2. The end segments were designed to include a hollow volume where a minimal amount of steel rebar reinforcement, concrete, and anchors were placed to resist localized bursting stresses from the post-tensioning. Since the end segment geometry was designed to include these simple hollow volumes, mainly requiring continuous toolpaths, each took approximately 10 minutes to print.

### 2.3. Final design

The final post-tensioned 3D printed, funicular concrete beam with embedded anticlastic geometry is 4.5 meters long, 1 meter wide at the bottom surface, and 0.4 meters deep at mid-span. The beam is made up of nine segments with eight ungrouted 1.27 cm diameter post-tensioned steel cables threaded throughout. The funicular concrete beam weighs about 1257 kg. Additional rebar cages and concrete were implemented to add reinforcement and strength in the anchorage zones at either end of the beam

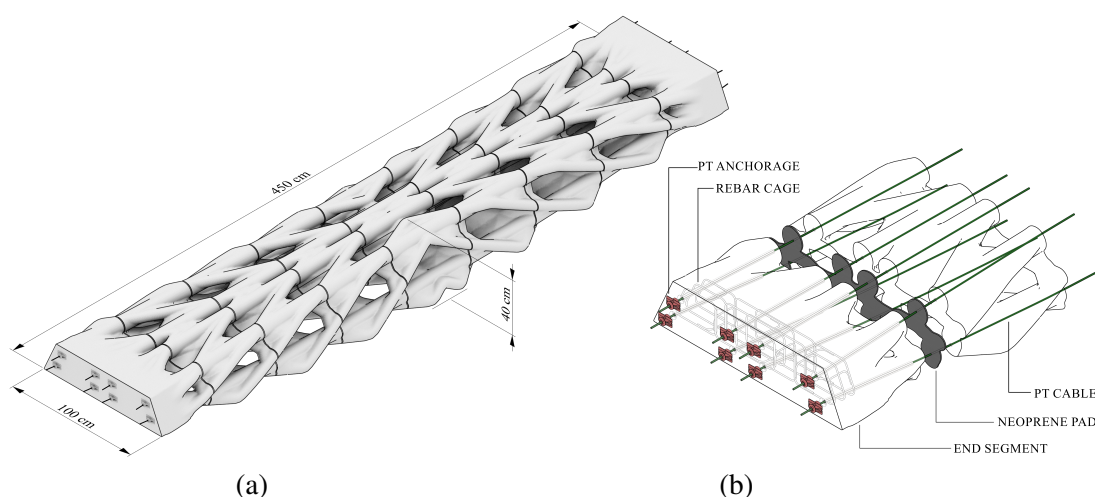


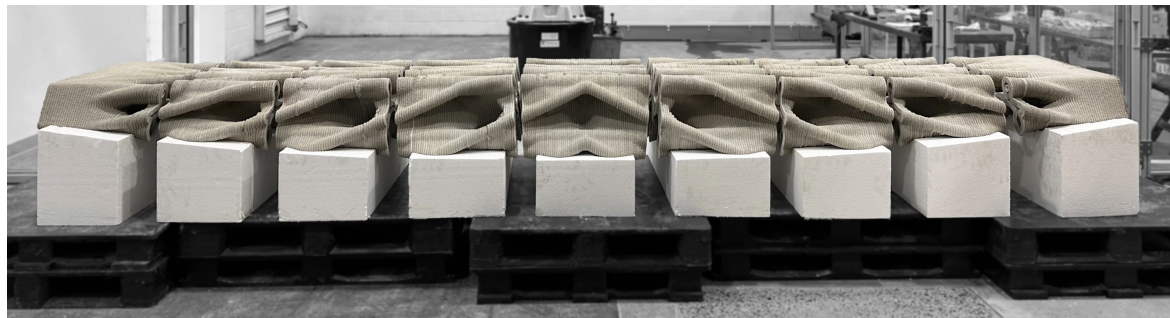
Figure 3: (a) Design of the prefabricated, post-tensioned funicular beam prototype. In consideration of construction and recyclability, the 4.5-meter-long structure is designed as a modular system, consisting of nine individual segments that are post-tensioned together. Each segment was 3D-printed using a multi-component concrete mix and with a multi-axis industrial robot arm. Each end segment was reinforced with additional material to resist bearing and bursting stress. (b) Detail of two modules, including concrete segments, neoprene pad at the interface, end-segment rebar cage, and post-tensioning anchors and cables.

to resist the bearing and bursting stresses developed during post-tensioning [11, 12]. An illustration of the final design is presented in Figure 3.

### 3. Assembly and post-tensioning

After all nine segments cured for 28 days, they were combined using post-tensioning steel cables to form the complete funicular beam. During the curing period, the end segments were further prepared by outfitting each with a steel rebar cage and filling the hollow volume with additional concrete. To ensure the modules are properly aligned for post-tensioning, robotically CNC-milled expanded polystyrene (EPS) foam blocks were used as temporary supports, importantly, these were easy to remove after assembly and could be reused for the construction of additional beams or repurposed. Each foam block was milled with a partial impression of its corresponding beam segment's bottom surface. The segments were placed on their respective block and moved to the appropriate location as shown in Figure 4(a). Once the segments were aligned, a 1.27 cm diameter post-tensioning cable was threaded through each of the eight channels, Figure 4(b). To lessen concentrated contact pressures caused by post-tensioning, 2.5 cm thick neoprene pads, cut to match each profile, were placed between each segment.

The beam was formed through post-tensioning of the nine individual segments properly aligned with steel cables threaded through each of the eight channels. Each cable was post-tensioned in increments of 150 MPa until the final desired force was reached, Figure 4(c). To further avoid applying too much force in any one particular cable, causing eccentric loading, a specific post-tensioning procedure was followed. The middle cables were post-tensioned first. Then the post-tensioning force was applied to the bottom outer two cables, followed by the top outer two cables. At the end of the post-tensioning process, the top four cables were post-tensioned to 300 MPa and the bottom four cables to 600 MPa, as determined by preliminary finite element analysis results. The larger post-tensioning force was applied to the bottom cables based on the determination of tensile force development using the geometric-based design method. A lesser post-tensioning force was applied to the top cables since compressive forces



(a) Assembly



(b) Threading cables



(c) Post-tensioning



(e) Final construction

Figure 4: Construction of the 4.5-meter funicular concrete beam prototype with embedded anticlastic surfaces, diamond geometry. (a) Nine 3D concrete printed segments temporarily supported on CNC-milled EPS foam blocks to ensure channels for post-tensioning are aligned. (b) Steel cables threaded through the structure's channels. (c) Post-tensioning of the steel cables, compressing the segments together, and forming the structure. (e) The final concrete 3D-printed, post-tensioned funicular beam prototype spanning and supporting its self-weight, notably resting on just two EPS foam blocks.

develop at the top surface of the beam during loading. Hence, the stressed top cables serve to provide an additional means for joining the segments.

Notably, the neoprene pads placed in between the segments achieved their intended purpose during the post-tensioning process, preventing fracture of the edges of the concrete segments pressing against each other. After being post-tensioned, the beam was elevated and the foam blocks between the end segments were removed. Prior to placing on designated test supports, the 4.5-meter-long funicular beam was bearing its own self-weight, Figure 4(d).

## 4. Four-point bending test

### 4.1. Test setup

A four-point bending test was conducted to investigate the flexural strength and ultimate load-bearing capacity of the funicular concrete beam prototype. The test setup included a 156 kN hydraulic actuator mounted to a loading frame, see Figure 5. The actuator was attached to a spreader beam that contacted two hollow structural sections (HSS), distributing the applied load to two regions on the beam. Specifically, each HSS was placed 1.71 meters from either end of the beam. To elevate the beam off the ground



(a) Test setup



(b) Load detail



(c) Support detail

Figure 5: Four-point bending test setup. (a) The setup consisted of a hydraulic actuator mounted to a steel frame. (b) The actuator was attached to a web-stiffened spreader beam that transferred the applied load to two hollow steel sections. (c) Two pin supports were placed on both ends of the beam constructed from steel beveled plates placed on solid round stock. Neoprene was placed between the concrete beam and the hollow sections, as well as the beveled plates at the supports. The funicular concrete beam prototype was spray-painted white prior to the test to assist in identifying cracks.

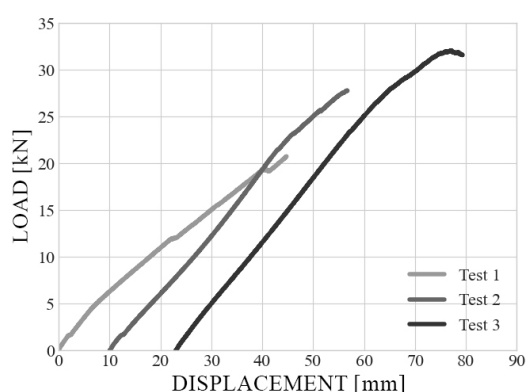
two additional HSSs were attached and placed underneath the supports at either end, as well as bolted to the strong floor, lifting the beam about 24 cm. Pin supports were constructed by placing a beveled steel plate on solid steel round stock. Placed at both ends of the beam, the beveled plate on round stock allowed for the beam to rotate at either end, but prevented horizontal and vertical translations. To evenly distribute the load application and minimize stresses developed between the funicular concrete beam with the loading and support setups, additional neoprene pads, 2.5 cm thick, were placed at each contact point. Details of the test setup, including both the load application and support configurations, are shown in Figure 5(b) and (c).

## 4.2. Results

The load-displacement curves for three test cycles conducted on the same funicular concrete beam are reported in Figure 6(a). An unfactored dead load of 12.33 kN and a live load of 5 kN/m<sup>2</sup> were considered as the beam's design code load level [5]. In total, the considered service load amounted to 23.6 kN, where the top surface of the beam has approximately a 2.25 m<sup>2</sup> area.

For the first cycle, the service load was applied to the beam. At approximately 12 kN a crack was initiated at the top surface of one of the segments adjacent to one of the end segments. The stiffness of the beam decreased from 0.47 kN/mm to 0.43 kN/mm at this point; however, a linear relationship continued until a second crack formed at a similar location on the next immediate segment. The test was stopped when the service load was achieved.

The next two cycles pushed the beam beyond the service load. For the second cycle, a linear stiffness of 0.72 kN/mm was determined. The initial two cracks continued to expand and propagate towards the middle segment during this test. However, no significant cracks were observed on the opposite segments or at the bottom surface of the beam. For the third cycle, the applied load was increased until the force value dropped, indicating the peak, ultimate load. The applied force reached 32.1 kN before continuously decreasing. The elastic stiffness was determined to be 0.68 kN/mm. At this load, the beam displaced 77 mm, and significantly deep cracks developed throughout the system, Figure 6(b). The beam collapsed to the floor ten minutes after unloading.



(a)



(b)

Figure 6: Force-displacement results of the funicular concrete beam under four-point bending. (a) The displacement was recorded at the mid-span of the beam. Three cycles were conducted on the same structure. After each cycle, the displacement of the structure at mid-span was recorded and used to adjust the data. The ultimate load-bearing capacity of the beam is 32.1 kN. (b) Cracks developed at the ultimate load-bearing capacity after the third test cycle.

### **4.3. Discussion**

The 4.5-meter-long modular, funicular concrete beam was capable of bearing 32.1 kN of load prior to reaching its ultimate load-bearing capacity. Notably, the beam has minimal mass and reinforcement, with just eight post-tensioning cables threaded throughout the system as the main reinforcement. While cracks formed during the first cycle, the beam continued to resist the applied load for the subsequent two cycles with a greater stiffness. In part, this behavior is a result of the post-tensioned cable reinforcement not yielding and compressing the segments together again during unloading. The increase in stiffness can also be attributed to the neoprene between each segment being compressed followed by the engagement of the concrete segments as well as the post-tensioning cables. When the neoprene was fully compressed near the top surface of the beam, the concrete segments engaged with each other providing additional rigidity, increasing the beam's stiffness. Overall the intended purpose of the neoprene was to lessen the concentrated stresses developed on the anticlastic surfaces between segments during the post-tensioning and serve to ensure the recyclability of the beam. As indicated by the stiffness increase, the displacement can be attributed to both the modular post-tensioned design and use of neoprene at the interfaces.

Throughout the test, it was noted that the beam's segments separated from each other at the bottom surface as the load increased. This separation indicates that the top region of the beam experienced compressive forces throughout the test, while the bottom region was not engaged. The beam's segments are held together by their interlocking geometry, threaded cables, and the post-tensioning forces compressing them. There is no bonding material directly fusing them, such as glue, ensuring that they are engaged. The separation of the segments at the bottom region also indicates why cracks formed on the top surface of the beam, due in part to the compressive forces, and not on its bottom region, in which the concrete did not develop tensile forces.

### **4.4. Recyclability**

The prefabricated modular, ungrouted assembly allows for the beam to be disassembled, readily separating concrete and steel construction materials to be recycled with minimal effort. After the structural test was completed, the post-tensioning cables were first removed from the beam, allowing the segments to be separated as well as all additional materials used in its construction (Figure 7). The combined design, fabrication, and construction approaches ensure sustainable practices by achieving desired performance with reduced construction materials that can be effectively separated and recycled/reused.



Figure 7: After testing, the modular funicular beam was disassembled efficiently and effectively. Since the beam was formed using ungrouted post-tensioning, the steel cables were readily removed from the concrete segments as well as all other construction materials, including the neoprene pads, post-tensioning anchors and wedges, all of which can be recycled.

## 5. Concluding remarks

In this paper, the design, fabrication, assembly, and structural testing of a funicular concrete beam prototype are presented. The beam prototype, designed using a comprehensive computational method, directly considers both compression and tensile forces through its funicular geometry and utilizes the optimized load path to inform the placement of post-tensioning cables and the embedment of periodic anticlastic surfaces. The design process also considers fabrication and assembly constraints due to constructability, for example, considerations with respect to concrete 3D printing and post-tensioning. The overall design and prefabrication strategy reduces the amount of materials needed for construction by minimizing reinforcement, reducing overall concrete use, and requiring no formwork. The segmentation of the beam also allows for the beam to be readily disassembled, reused, or recycled.

Since this type of prefabricated concrete beam, with minimal post-tensioning reinforcement and embedded anticlastic surfaces, has not been studied before, a four-point bending test was performed to determine its strength and stiffness. The ultimate load-bearing capacity of the beam was determined to be 32.1 kN. While cracks formed during the test, the overall stiffness of the beam did not reduce. The beam's stiffness increased during the subsequent tests, in part due to post-tensioning cables continuing to compress the segments after unloading and the neoprene placed between the segments. The beam was capable of bearing a load greater than the estimated service load. When the ultimate load-bearing capacity was reached, the failure of the beam was not sudden. The beam was able to support its own weight several minutes after the test before collapsing.

This work served as a proof-of-concept for prefabricated, modular funicular structures and will inform the redesign and continued testing of similar and larger spanning, prefabricated structures with minimal reinforcement. The current test results can be used to develop and calibrate finite element models to closely approximate the behavior of such systems with complex geometries, segmentation, and post-tensioning. Additional developments to the construction process can also be explored, such as finding alternatives to neoprene with the intent of engaging the bottom surface of the beam, while ensuring sustainable practices are continued.

## Acknowledgments

The authors acknowledge the support provided by the Advanced Research Projects Agency Energy (ARPA-E) Grant of the U.S. Department of Energy (DE-AR0001631). This research was also partially funded by the National Science Foundation CAREER Award (NSF CAREER-1944691 CMMI) and the National Science Foundation Future Eco Manufacturing Research Grant (NSF, FMRG-CMMI 2037097) awarded to Masoud Akbarzadeh.

## References

- [1] M. Akbarzadeh, H. Chai, Y. Zhi, M. E. Ororbia, T. Teng, M. Bernhard, D. Bolhassani, F. Yavartanoo, J. Tapia, K. Pajak, M. Bernard, L. Troussset, P. Kassabian, and B. Waligun, "Diamanti: 3d-printed, post-tensioned concrete canopy," in *FABRICATE 2024: Creating Resourceful Futures*, UCL Press, 2024, pp. 292–301.
- [2] H. Chai, Y. Lu, M. Hablicsek, and M. Akbarzadeh, "Generation of a compression-tension combined funicular polyhedral beam structure," in *Proceedings of IASS Annual Symposia*, International Association for Shell and Spatial Structures (IASS), 2023, pp. 1–11.
- [3] M. Akbarzadeh, "3d graphic statics using polyhedral reciprocal diagrams," Ph.D. dissertation, ETH Zürich, Zürich, Switzerland, 2016.

- [4] J. Lee, “Computational design framework for 3d graphic statics,” Ph.D. dissertation, ETH Zurich, Department of Architecture, Zurich, 2018. DOI: 10.3929/ethz-b-000331210.
- [5] European Union, *Eurocode 1. Actions on Structures - Traffic Loads on Bridges (EN 1991-2:2003 (E))*. European Committee for standardization, 2003. [Online]. Available: <https://www.phd.eng.br/wp-content/uploads/2015/12/en.1991.2.2003.pdf>.
- [6] H. A. Schwarz, “Ueber die minimalfläche, deren begrenzung als ein von vier kanten eines regulären tetraeders gebildetes räumliches vierseit gegeben ist,” *Monatsberichte der Königlichen Akademie der Wissenschaften zu Berlin*, pp. 149–153, 1865.
- [7] A. H. Schoen, *Infinite periodic minimal surfaces without self-intersections*. National Aeronautics and Space Administration, 1970, vol. 5541.
- [8] M. Bernhard, M. Hansmeyer, and B. Dillenburger, “Volumetric modelling for 3D printed architecture,” in *AAG - Advances in Architectural Geometry*, L. Hesselgren, A. Kilian, O. Sorkine Hornung, S. Malek, K.-G. Olsson, and C. J. K. Williams, Eds., Göteborg, Sweden: Klein Publishing GmbH, 2018, pp. 392–415, ISBN: 978-3-903015-13-5. [Online]. Available: <https://research.chalmers.se/en/publication/504188>.
- [9] J. F. Blinn, “A Generalization of Algebraic Surface Drawing,” *ACM Transactions on Graphics*, vol. 1, no. 3, pp. 235–256, 1982, ISSN: 07300301. DOI: 10.1145/357306.357310. [Online]. Available: <http://portal.acm.org/citation.cfm?doid=357306.357310>.
- [10] M. Bernhard, M. Bolhassani, and M. Akbarzadeh, “Performative Porosity – adaptive infills for concrete parts,” in *Proceedings of the IASS Annual Symposium 2020/21*, Surrey, UK, 2021.
- [11] P.-T. Institute, *Post-tensioning manual*. Post-Tensioning Institute, 1985.
- [12] K. D. Bondy and B. Allred, *Post-Tensioned Concrete: Principles and Practice*. Lulu. com, 2017.